Numerical Methods in Civil Engineering, 10-2 (2025) 12-26

Numerical Methods in Civil Engineering

Journal Homepage: https://nmce.kntu.ac.ir/

Influence of Shear Damper Arrangement on Seismic Performance of Mid-Rise Steel Framed Buildings

Amir Shirkhani [*], Ahmed Elgammal [**], Yasmin Ali [***]

ARTICLE INFO

RESEARCH PAPER

Article history:
Received:
September 2025
Revised:
November 2025
Accepted:
December 2025

Keywords:
Damper placement;
Eccentrically Braced Frame (EBF);
Energy Dissipation;
Stainless Steel;
Shear Link

Abstract:

Strategic damper placement is critical for optimizing the seismic performance of steel buildings, yet the optimal arrangement for eccentrically braced frames (EBFs) remains a key research question. This study investigates this issue by evaluating the effectiveness of stainless-steel longitudinally stiffened vertical shear links (LVSLs). A ten-story steel frame was designed in four distinct configurations: a benchmark moment-resisting frame (MRF) and three EBFs with distinct LVSL arrangements, where the primary variations were concentrated in the lower stories. The seismic response of each configuration was assessed using nonlinear static pushover and dynamic time history analyses. The results demonstrate that all EBF configurations exhibit superior performance over the MRF in terms of lateral stiffness, strength, and ductility. A configuration that concentrated two smaller LVSLs in each of the first three stories displayed the most favorable response, yielding significant reductions in interstory drift and superior energy dissipation under both design-basis (DBE) and maximum considered earthquake (MCE) scenarios. While EBF systems require more structural steel than MRF systems, the proposed optimal configuration achieved this enhanced performance while utilizing the lowest total mass of stainless-steel dampers. This outcome demonstrates that for EBF systems, a concentrated damper arrangement tailored to the distribution of seismic demand provides a more resilient and materially efficient solution than generalized distributed placement strategies.

NOTATIONS

α	Post-yield stiffness ratio
$u(t)$	Shear deformation
$\dot{u}(t)$	Rate of deformation
$z(t)$	Hysteretic variable
k	Initial stiffness
F_y	Yield force
T	Fundamental period
M_{eff}	Participating mass ratio
D	Roof displacement
H	Total building height
K	Elastic lateral stiffness
F_u	Ultimate strength

* *Corresponding Author: Assistant Professor, Department of Civil Engineering, University of Torbat-e Jam, Torbat-e Jam, Iran. https://orcid.org/0000-0003-2532-2906; Email: shirkhani@tjamcaas.ac.ir*
** *Department of Civil Engineering, Sichuan University, Chengdu 610065, China. https://orcid.org/0000-0002-4144-667X*
*** *Department of Civil Engineering, Sichuan University, Chengdu 610065, China. https://orcid.org/0000-0001-7413-0885-Department of Civil Engineering, Delta University for Science and Technology, Gamasa 11152, Egypt.*

1. Introduction

The design of multi-story steel buildings in seismic regions requires lateral force-resisting systems capable of managing large inelastic deformations while controlling story drifts [1,2]. Among the established solutions, moment-resisting frames (MRFs) provide significant ductility and structural redundancy through the flexural yielding of beams and columns, offering considerable architectural flexibility [3,4]. However, their inherent flexibility often results in larger lateral displacements, which can pose challenges for drift-sensitive components and overall building performance [5]. In contrast, braced frames achieve superior lateral drift-sensitive components and overall building performance [5]. In contrast, braced frames achieve superior lateral stiffness and strength primarily through the axial action of diagonal members, providing an efficient means of controlling lateral drift [3,4]. These braced systems are broadly classified into concentrically braced frames (CBFs), which are highly

https://doi.org/10.61882/NMCE.2509.1101

efficient in terms of stiffness but may offer limited post-yield ductility, and eccentrically braced frames (EBFs). EBFs were developed to strategically combine the high stiffness of a braced system with the stable energy dissipation capacity of a ductile MRF by isolating inelastic activity within a designated shear link [4]. This configuration allows the main structural members to remain essentially elastic while the link yields, providing a reliable energy dissipation mechanism. To further refine performance, dual systems that integrate MRFs with various types of braced frames have also been explored to leverage the distinct advantages of each system type [3,6]. The emergence of systems like buckling-restrained braced frames has also offered new pathways for achieving robust seismic performance [7].

The principle underlying the EBF design, where inelasticity is intentionally confined to a specific element, is a foundational concept in passive energy dissipation. Such systems enhance seismic resilience by incorporating devices engineered to absorb and dissipate a significant portion of the input earthquake energy, thereby protecting the primary structural frame. Metallic hysteretic dampers, a prominent category of these devices, are designed to undergo controlled yielding cycles, which serves to limit forces transferred to the rest of the structure and prevent premature failure of critical members [8,9].

The integration of these passive control systems offers a reliable method for managing seismic response. Research has shown that hysteretic dampers can be designed to effectively control maximum interstory drifts and regularize the distribution of stiffness and strength along the building's height [10,11]. By concentrating damage within these specialized, often replaceable components, the system preserves the integrity of its main load-bearing elements, which are intended to remain essentially elastic [12]. The shear link within an EBF is a quintessential example of this strategy, functioning as an integrated hysteretic damper that provides stiffness under service loads and reliable energy dissipation during a severe earthquake [13,14].

Despite their effectiveness, conventional steel shear links are susceptible to several performance limitations and failure modes that can compromise their intended ductile behavior. The geometric design of the link itself presents a fundamental challenge; short links, while efficient at dissipating energy, accommodate large inelastic rotations that can damage adjacent non-structural components, whereas longer links tend to exhibit reduced ductility [15]. Under severe cyclic loading, the link material is subjected to a combination of high shear and axial stresses, making it vulnerable to low-cycle fatigue and eventual fracture [16].

Furthermore, the performance of the entire system is highly sensitive to fabrication quality and connection detailing. Improperly executed or designed welds at the link connection to surrounding members can lead to brittle fractures, preventing the link from developing its full inelastic capacity and undermining the seismic resilience of the frame [17]. Moreover, at a system level, EBFs do not inherently guarantee a uniform distribution of interstory drift, with studies indicating a tendency for inelastic demand to concentrate in certain stories if link properties are not carefully controlled [18,19]. These vulnerabilities have motivated research into alternative designs, such as replaceable shear links and enhanced box dampers, to improve reparability and mitigate these failure modes [17,20].

In response to these performance vulnerabilities, significant research has been directed toward developing innovative link designs that enhance stability and energy dissipation. These efforts include the exploration of alternative materials or composite sections to increase shear capacity [21,22]. A particularly effective advancement has been the refinement of stiffening strategies to control web instability. While conventional links often rely on transverse stiffeners [23], a key innovation has been the implementation of longitudinal stiffeners. The efficacy of this approach is rooted in the prevention of premature web instability. Recent investigations on thin-walled steel sections have further affirmed that the strategic implementation of web stiffeners significantly enhances load-bearing capacity by delaying the onset of local buckling under combined shear and bending actions [24,25]. Recent investigations have demonstrated that longitudinally stiffened vertical shear links exhibit superior performance, providing enhanced strength, ductility, and energy dissipation capacity compared to their transversely stiffened counterparts [14,26]. By effectively delaying web buckling, the longitudinal stiffeners enable the link to undergo greater inelastic deformations, thereby enhancing its contribution to the structure’s overall seismic resilience. Such component-level improvements are essential for advancing the robustness and reliability of braced frame systems.

Selecting a suitable material is also crucial to optimizing damper performance, as certain grades of stainless steel provide distinct mechanical advantages over conventional carbon steel. Austenitic stainless steels, in particular, are characterized by a superior combination of high ductility and significant strain hardening, which allows their strength to increase substantially as they deform [27]. Furthermore, the material's high ductility is associated with favorable low-cycle fatigue characteristics, a critical attribute for components designed to undergo repeated inelastic deformations [28–30]. This property is complemented by pronounced cyclic hardening, a behavior that differs significantly from that of carbon steel and allows the material's resistance to increase over repeated loading cycles [31]. This phenomenon has been recently verified in specific

alloys such as AISI 316L, where the accumulation of microstructural dislocations under repeated loading progressively enhances the material's strength and resistance to deformation [32,33]. Consequently, dampers fabricated from suitable stainless steel alloys can exhibit greater ultimate strength and energy dissipation capacity [34]. While this response is dependent on the specific grade and loading history, the inherent hardening characteristics make stainless steel a highly promising material for the dissipative zones of seismic-resistant elements like shear links. Although the mechanical advantages of stainless-steel longitudinally stiffened vertical shear links (LVSLs), particularly their superior buckling resistance and energy dissipation, are increasingly acknowledged at the component level, how these benefits translate to the performance of the entire structural system remains an open question. This is a critical consideration, as recent research has consistently demonstrated that the vertical distribution of dampers is a primary factor governing a structure's global energy dissipation capacity and overall seismic performance [35,36]. While recent studies on passive control systems often suggest that a vertically distributed damper arrangement is required to minimize interstory drift [37–39], the applicability of this principle to EBF systems, where shear links act as integral structural fuses and inelastic demand is inherently concentrated in the lower stories, has not been systematically investigated.

Consequently, this study bridges a critical gap between component-level advancements in shear link design and their optimal system-level implementation. It systematically investigates whether the conventional wisdom of distributed damper placement holds true for EBFs equipped with stainless-steel LVSLs, or if a concentrated arrangement tailored to the inherent distribution of seismic demand offers a more effective and efficient solution. The investigation focuses on a ten-story frame designed in four configurations: a benchmark moment-resisting frame (MRF) and three EBFs with distinct LVSL arrangements in the lower stories. By linking global performance metrics (stiffness, strength, drift uniformity, and energy dissipation) from nonlinear static and dynamic analyses to these specific placement strategies, this research offers crucial insights into resolving the known EBF issue of non-uniform drift. The novelty of this work lies in its specific focus on the system-level optimization of stainless steel LVSLs, which is a configuration that has not been previously investigated in multi-story frames. While prior optimization studies have focused on conventional carbon steel links, this research isolates the unique impact of the LVSL arrangement on global seismic response. By bridging component-level behavior with global performance metrics, the study demonstrates that a targeted damper concentration strategy can unlock the full potential of these advanced dissipative elements, offering a more resilient and materially efficient alternative to traditional designs.

2. Design and Modeling of Structural Configurations

The seismic performance of the proposed LVSL arrangements was evaluated through a systematic, multi-stage investigation. The complete research framework, encompassing the design of the prototype structures, the development of the analytical models, and the execution of a suite of nonlinear analyses, is graphically summarized in Figure 1. This process involved the design of four distinct structural configurations, followed by their implementation in a high-fidelity numerical model. The models were subsequently subjected to both nonlinear static and dynamic time history analyses to facilitate a comprehensive comparative assessment of their seismic performance.

2.1 Prototype Structures and Design Philosophy

The investigation focuses on a prototype ten-story, three-bay planar frame composed of S355 grade steel [40], with a uniform story height of 3 m and bay width of 6 m. Four distinct lateral force-resisting systems were modeled to facilitate a comparative analysis. The overall elevations of these configurations are illustrated in Figure 2 and include a benchmark MRF and three eccentrically braced frames (EBF1, EBF2, and EBF3). The EBF models incorporate stainless-steel LVSLs, which are the focus of this study. To provide clarity on this key component, a detailed schematic of the LVSL and its typical integration within a braced bay is presented in Figure 3. These specialized links are designed to act as ductile fuses, with longitudinal stiffeners enhancing their buckling resistance and energy dissipation capacity. The placement of these LVSLs is systematically varied across the EBF models, with modifications concentrated in the lower stories, as these regions typically experience the largest interstory drifts during a seismic event and are therefore critical zones for optimizing damper performance. The design of all four configurations adhered to EN 1998-1 [41] for seismic actions and EN 1993-1-1 [40] for steel structures, assuming uniform distributed dead and live loads of 24 kN/m and 12 kN/m on all beams. The building site corresponds to soil type C with a design peak ground acceleration of 0.2g. The MRF was designed using a multimodal response spectrum analysis to determine seismic demands and size the members accordingly. In contrast, the design of the EBF systems employed a capacity design philosophy. This process involved first sizing the LVSLs based on story shears derived from a response spectrum analysis, following procedures recently developed by Elgammal and Ali [26]. Subsequently, the beams, columns, and braces were designed with sufficient strength to resist

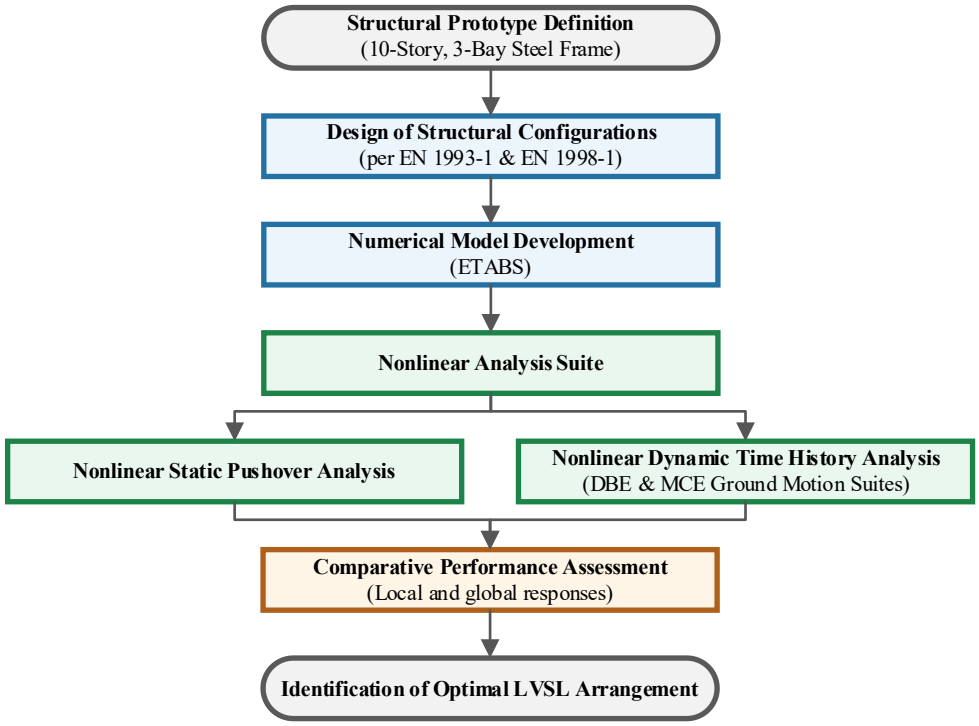

Fig. 1: Flowchart of the research methodology

the maximum forces generated when the LVSLs reach their full plastic capacity, ensuring that inelastic deformation is confined to the links. It is important to clarify that all configurations represent newly designed structures conforming to modern codes, not seismically deficient frames subjected to retrofit. The design characteristics of the LVSLs are summarized in Table 1. The design resulted in columns ranging from HE200B to HE400B for the MRF and from HE300B to HE340B for the EBFs. Diagonal braces in the EBF systems ranged from HE120B to HE160B, while all beams were HE200B. Complete cross-section details for these models are documented in [42].

A key outcome of this design process was that the primary structural columns in the EBF configurations were generally smaller than those in the MRF, as the braces and dampers contribute substantially to the required lateral stiffness and strength.

2.2 Details of the Numerical Model

Numerical models of the four configurations were developed using the finite element software ETABS [43], as illustrated in Figure 4(a). The analysis was constrained to two dimensions, with degrees of freedom restricted to the plane of the frame. This planar frame idealization is considered appropriate for this fundamental investigation, as it assumes a prototype building that is regular and symmetric in plan. For such a structure, the primary seismic response is dominated by translational modes, allowing for a clear comparative assessment of the damper arrangements without the confounding influence of torsion. A fixed-base condition was assumed at the foundation level, and the effects of soil-structure interaction were not considered.

The modeling process involved several key steps. First, beams, columns, and braces were modeled using linear frame elements. Second, to capture the inelastic behavior of the frame, a lumped plasticity approach was adopted by assigning nonlinear rotational hinges at the ends of beams and columns, as well as at the mid-span of braces. The force-deformation properties for these hinges, including parameters for immediate occupancy (IO), life safety (LS), and collapse prevention (CP), were explicitly defined according to the backbone curves specified in ASCE/SEI 41-17 [44]. A detailed view of these nonlinear assignments is shown in Figure 4(b).

Third, the stainless-steel LVSLs were modeled using specialized nonlinear 'Link/Support' elements. The hysteretic behavior for these elements was assigned to the shear degree of freedom (U2) and governed by the Wen plasticity model [43], which effectively captures the smooth transition from elastic to plastic response characteristic of metallic dampers [9,45,46]. The idealized bilinear force-deformation response of this model is illustrated in Figure 5. The total restoring force, $F(t)$, is defined as a function of the elastic stiffness, post-yield behavior, and an internal hysteretic variable:

$$F(t) = \alpha k u(t) + (1 - \alpha) F_y z(t) \quad (1)$$

where k is the initial elastic stiffness, $u(t)$ is the shear deformation, F_y is the yield force, and α is the post-yield stiffness ratio. The dimensionless internal variable, $z(t)$, governs the hysteretic shape and is bounded by $|z| \leq 1$, where $|z| = 1$ represents the yield surface. The evolution of $z(t)$ is governed by the following conditional differential equation:

$$\dot{z}(t) = \begin{cases} \frac{k}{F_y}\dot{u}(t)[1 - |z(t)|^m] & \text{if} \quad \dot{u}(t)z(t) > 0 \\ \frac{k}{F_y}\dot{u}(t) & \text{Otherwise} \end{cases} \tag{2}$$

In this formulation, $\dot{u}(t)$ and $z(t)$ are the rate of deformation and the hysteretic variable, respectively. The exponent m controls the sharpness of the transition from the elastic to the plastic range, with larger values producing a more acute yield corner. For this study, the key parameters defining the model (i.e., initial stiffness (k), yield force (F_y), and stiffness ratio (α)) were determined for each LVSL in accordance with the design methodology previously described, with the hysteretic shape parameters calibrated against the detailed component behavior documented in [26].

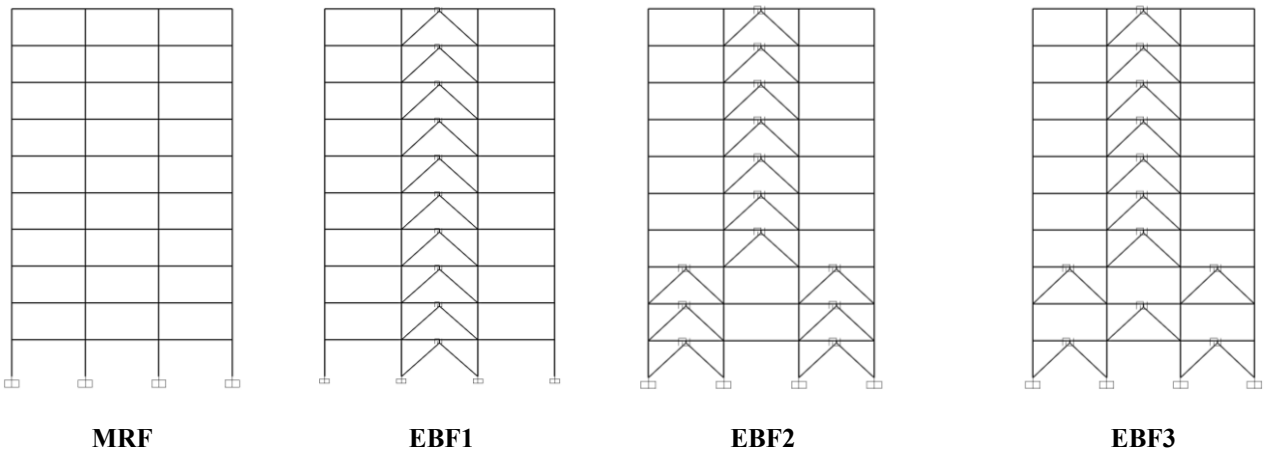

Fig. 2: Elevation view of building configurations

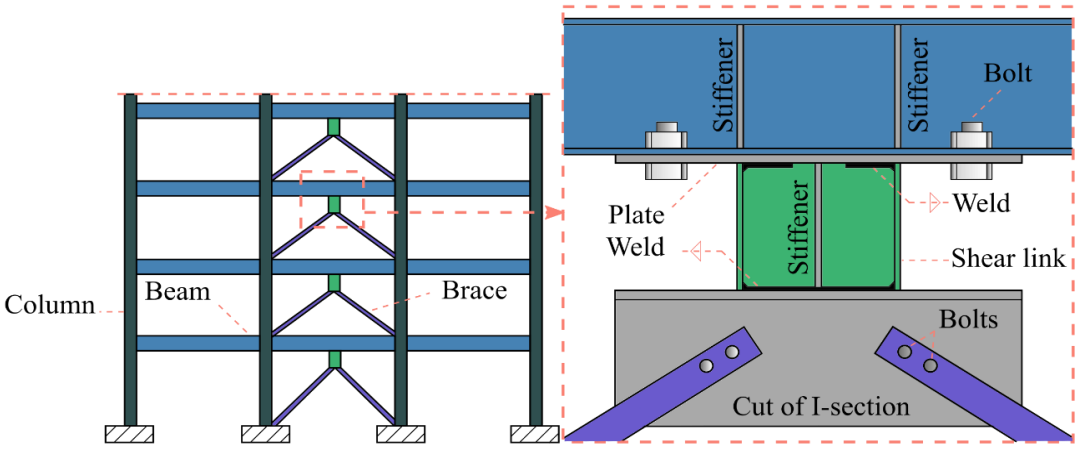

Fig. 3: Schematic of the LVSL and its integration within the eccentrically braced frame

Table 1: Characteristics of stainless-steel LVSLs (where n denotes the number of LVSLs per story and e is the length of each LVSL in mm)

Story	EBF1			EBF2			EBF3		
	n	e (mm)	Section	n	e (mm)	Section	n	e (mm)	Section
1	1	250	IPE120	2	170	IPE80	2	170	IPE80
2	1	250	IPE120	2	170	IPE80	1	250	IPE120
3	1	250	IPE120	2	170	IPE80	2	170	IPE80
4-6	1	210	IPE100	1	210	IPE100	1	210	IPE100
7-10	1	170	IPE80	1	170	IPE80	1	170	IPE80

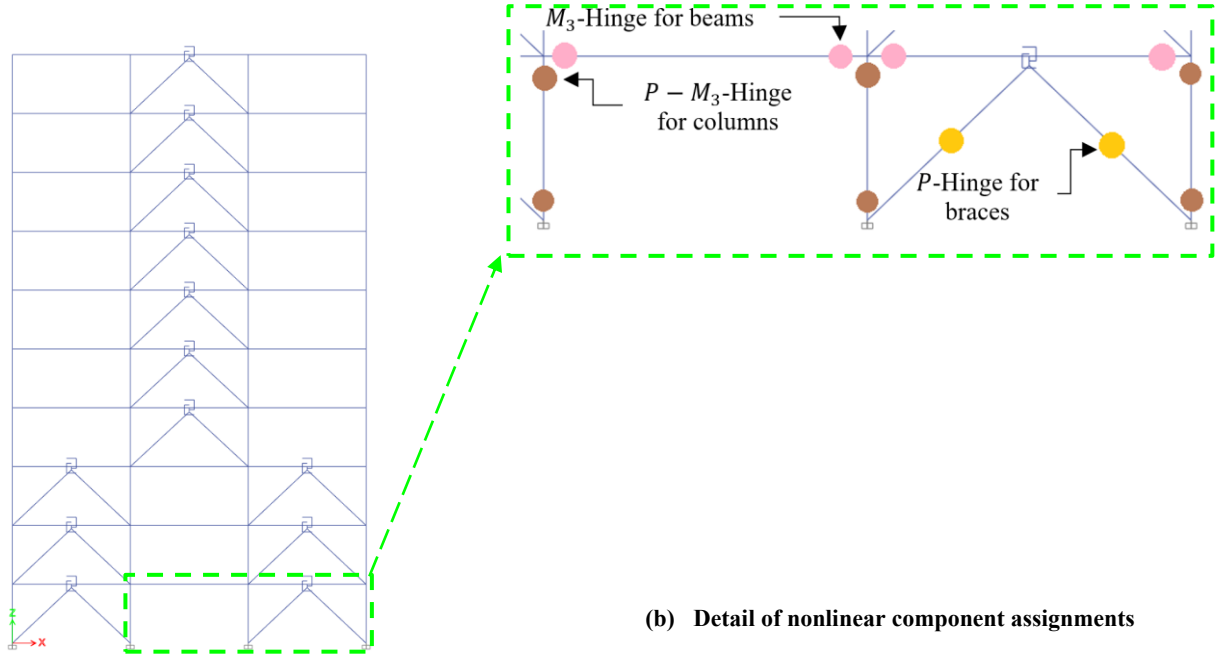

(a) Overall representative model (EBF-2)

(b) Detail of nonlinear component assignments

Fig. 4: Implementation of the numerical model in ETABS [43]

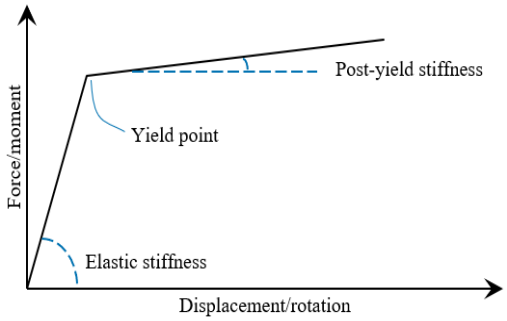

Fig. 5: Idealized bilinear response of the Wen plasticity model used for LVSL dampers

An initial modal analysis was performed to characterize the dynamic properties of each configuration. The fundamental periods (T) and associated participating mass ratios (M_{eff}) for the first three modes are presented in Table 2. Despite being composed of larger structural sections, the MRF exhibits a longer fundamental period (1.04 s) than any of the EBF models (0.93–0.94 s). This confirms that the inclusion of bracing and LVSLs provides the EBF systems with significantly greater lateral stiffness, a property that compensates for their comparatively smaller primary members. The LVSL arrangement has a minor influence on the fundamental period; however, the EBF3 configuration exibits a slightly longer period than EBF1 and EBF2, suggesting a marginal reduction in overall stiffness. For all configurations, the cumulative mass participation of the first three modes exceeds 90%, confirming their sufficiency for capturing the dominant dynamic response in subsequent analyses.

Table 2: Fundamental periods (T) and mass participation (M_{eff})

Mode	MRF		EBF1		EBF2		EBF3	
	T (s)	M_{eff} (%)	T (s)	M_{eff} (%)	T (s)	M_{eff} (%)	T (s)	M_{eff} (%)
1	1.04	73.3	0.93	75.8	0.93	75.4	0.94	75.1
2	0.35	11.6	0.30	11.0	0.30	11.1	0.32	11.3
3	0.18	5.3	0.16	4.80	0.16	4.80	0.16	4.82
Σ	-	90.2	-	91.6	-	91.3	-	91.2

2.3 *Numerical Model Validation*

To explicitly verify the accuracy of this numerical approach, it was validated against the experimental results of Lian and Su [47]. They tested two single-story eccentrically braced frames with Q460 steel members and Q345 steel shear links (length = 0.5 m). The specimens, with a bay width of 3.6 m and height of 1.8 m, were subjected to monotonic and cyclic lateral loading under 400 kN column axial loads. Cross-

sectional dimensions followed H-shaped profiles for beams (H225×125×6×10), columns (H150×150×6×10), braces (H125×120×6×10), and shear links (H225×125×6×10). Since mechanical parameters for the shear links were not provided in the experimental study, these were derived via auxiliary finite element analysis in ANSYS [48] and implemented in ETABS [43] using the Wen plasticity model [49]. To replicate the experimental conditions, a single-story ETABS model was created using the specified member sections and material properties, with the 400 kN column axial loads applied and the lateral loading protocol simulated directly. Comparison of numerical and experimental results (Figure 6) revealed close agreement, though the numerical curves exhibited marginally higher stiffness and strength. Yield and ultimate base shear ratios (experimental/numerical) ranged from 0.92–1.08 and 0.93–0.97, respectively, with elastic stiffness ratios of 0.84 (monotonic) and 0.93 (cyclic). The consistency in load-capacity predictions and hysteretic response confirms the model's efficacy in simulating shear link behavior under both static and dynamic loading regimes.

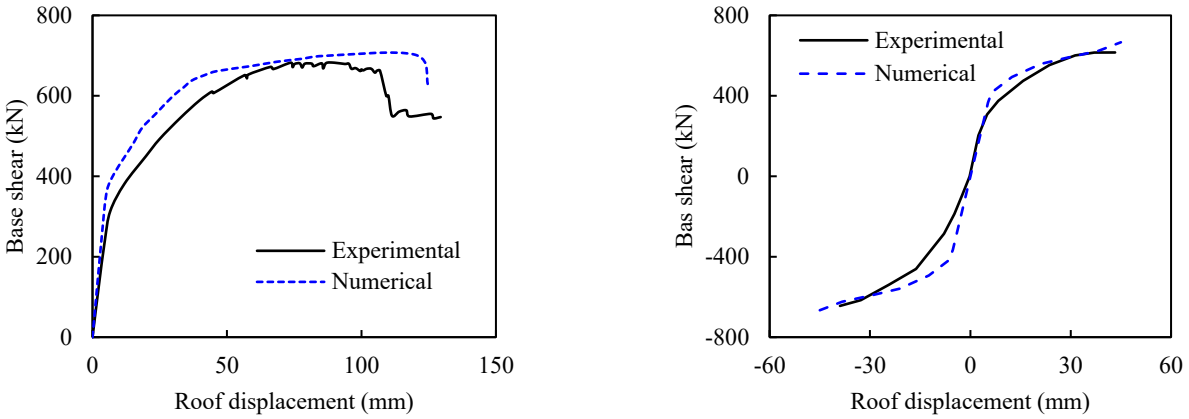

Fig. 6: Comparison of experimental results from Lian and Su [47] and numerical simulations in ETABS [43], showing the pushover curve for monotonic loading and the backbone (skeleton) curve for cyclic loading

3. Nonlinear Static Pushover Analysis and Performance Assessment

To evaluate the inelastic capacity of the four structural configurations, a nonlinear static pushover analysis was performed by applying a monitored lateral displacement to the roof up to a target drift ratio (D/H) of 3%, as recommended for collapse assessment [47], where D denotes the roof displacement and H is the total building height. The resulting force-displacement relationships, plotted in Figure 7, demonstrate that all EBF configurations exhibit substantially improved performance over the benchmark MRF. The EBF systems achieve higher lateral strength and initial stiffness, indicating a more robust response under increasing lateral loads. The extended elastic range seen in the pushover curves, with a nearly linear response up to a roof drift ratio (D/H) of approximately 0.3%, is characteristic of modern systems designed to stringent code-based drift limits. This behavior reflects the high initial stiffness provided by the bracing elements and capacity-designed members, which are intended to delay significant global yielding until the LVSLs are fully engaged. Among the braced frames, the EBF2 configuration, which concentrates dampers in the lowest stories, shows the earliest initiation of yielding in its shear links. This early activation of the energy dissipation mechanism is advantageous, as it protects the primary structural members from inelastic demand sooner. The EBF1 configuration also performs well, whereas the EBF3 model, with its staggered damper arrangement, shows a comparatively less favorable response. A quantitative comparison of key performance metrics derived from the pushover analysis is presented in Table 3.

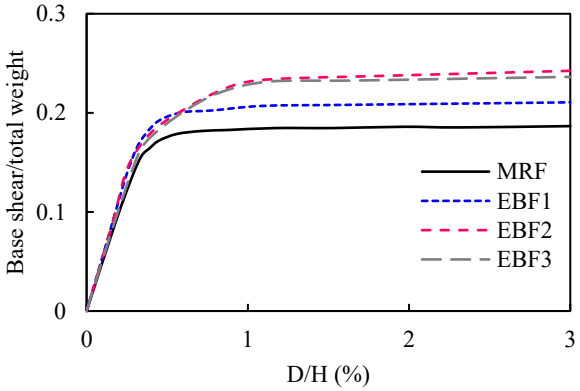

Fig. 7: Combined pushover curves of all configurations

Table 3: Key performance metrics from pushover analysis

Configuration	K (kN/mm)	F_u (kN)	F_{IO} (kN)	F_{LS} (kN)	F_{CP} (kN)
MRF	10.8	1261	1172	1245	1259
EBF1	12.2	1424	1334	1393	1414
EBF2	12.3	1625	1354	1590	1617
EBF3	11.5	1590	1295	1567	1583

The elastic lateral stiffness (K) of the EBF configurations is between 6% and 14% greater than that of the MRF. It is important to note that the global initial stiffness is a system-level property influenced by the arrangement of all dampers, not merely their quantity in the lowest story. For instance, the initial stiffness of EBF2 (12.3 kN/mm) is nearly identical to that of EBF1 (12.2 kN/mm). While EBF2 incorporates two LVSLs in each of the first three stories, these links are geometrically smaller (IPE80, $e = 170$mm) compared to the single, more substantial link in EBF1 (IPE120, $e = 250$mm), as detailed in Table 1. The combined stiffness of the two smaller links thus approximates that of the single larger one. Conversely, the EBF3 configuration exhibits a slightly lower global stiffness (11.5 kN/mm) due to its staggered damper layout. The presence of a less-stiff second story between two stiffer stories introduces a vertical irregularity that reduces the overall system's initial elastic resistance. In terms of ultimate strength (F_u), the EBF systems demonstrate a significant advantage, with capacities 12% to 22% higher than the MRF. The EBF2 and EBF3 configurations achieve the highest ultimate strengths, suggesting superior load-bearing capacity. Furthermore, despite having smaller primary structural members, all EBF configurations exhibit a higher ductility index (μ) than the MRF. This finding underscores the effectiveness of confining inelasticity to the ductile LVSLs, which enhances the overall deformation capacity of the system. The distribution of plastic hinges at the 3% roof drift level, shown in Figure 8, reveals the underlying failure mechanisms. The MRF develops numerous plastic hinges in its beams and at the base of its columns, with many reaching the CP performance level. In contrast, the EBF configurations concentrate inelastic demand within the LVSLs, which allows the primary beams and columns to remain largely within the LS performance level or below. In the same vein, the LVSL dampers at this drift magnitude are within their CP rotation limits, thereby validating their role as the primary energy dissipation mechanism. This confirms that the capacity design approach successfully protects the main structural system. The strategic placement of LVSLs also had a pronounced effect on drift control, as shown by the maximum interstory drift profiles at the collapse prevention limit state in Figure 9. All EBF systems maintained significantly lower interstory drifts than the MRF. The EBF1 and EBF2 configurations produced the most desirable drift distributions, which were both smaller in magnitude and more uniform over the building's height. Conversely, the staggered damper arrangement in the EBF3 model resulted in a notable concentration of interstory drift in the third story, an undesirable response caused by the abrupt change in stiffness at that level. A key reason for the EBFs' superior performance is the significant contribution of the LVSLs to resisting story shear. At a roof drift of 1%, the LVSLs in the ground floor carried approximately 76% of the total story shear, and even at 3% drift, they continued to resist an average of 56%. This substantial shear resistance provided by the dampers effectively unloads the columns, mitigating damage and controlling drift.

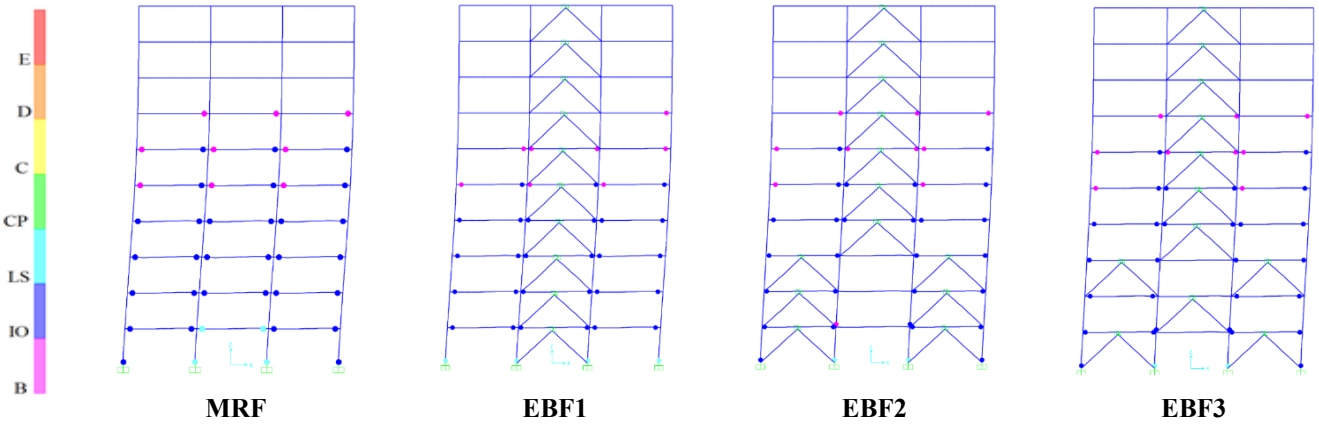

Fig. 8: Plastic hinge distribution at 3% roof drift. Note: The colored markers indicate the performance state of frame members; the LVSL dampers are functioning as structural fuses within the CP limit state

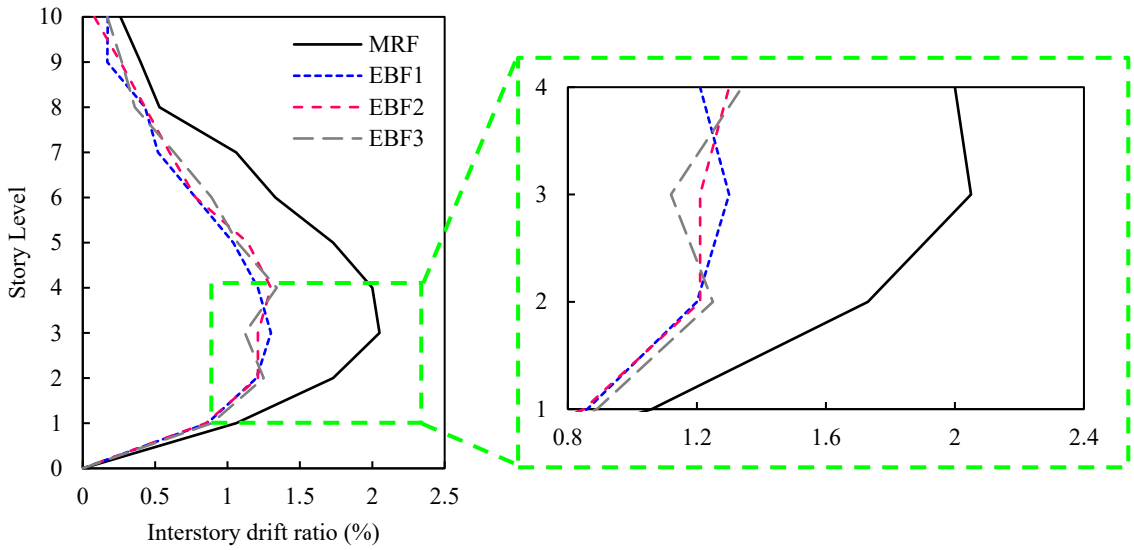

Fig. 9: Maximum interstory drift ratios at collapse prevention performance level

4. Nonlinear Dynamic Response under Design-Basis Earthquakes

To assess performance under realistic seismic loading, nonlinear time history analyses were conducted using a suite of ground motions (Table 4). The selected records were spectrally matched to the design response spectrum specified in EN 1998-1 [41] for soil type C, ensuring consistency with the design-basis earthquake (DBE) level. This matching process, performed using the wavelet algorithm implemented in SeismoMatch [50], adjusts the frequency content of the records to align with the target spectrum [51], as illustrated in Figure 10, and provides a uniform basis for comparing the dynamic response of the four configurations.

Table 4: Characteristics of the selected ground motions

Ground motion	Station	Component	Frequency range	Peak ground acceleration (g)
El Centro 1940	Imperial Valley	EW	0.02-25.0	0.32
Taft 1952	Lincoln School	N21E	0.01-50.0	0.16
Northridge 1994	Sepulveda Blvd	EW	0.02-50.0	0.57
Loma Prieta 1989	Sewage Plant	EW	0.09-50.0	0.37
Chi Chi 1999	Taichung	EW	0.01-50.0	0.36

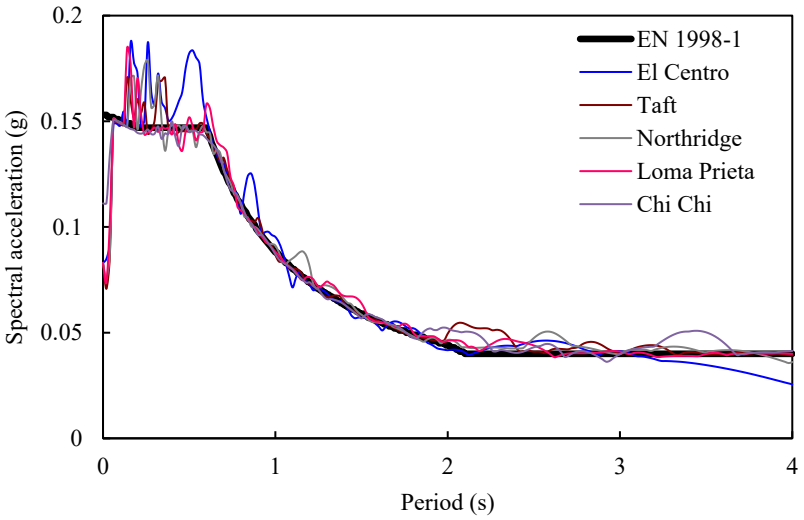

Fig. 10: Target and matched response spectra for selected ground motions

Figure 11 compares the roof displacement time histories of all four configurations (MRF, EBF1, EBF2, EBF3) under the

Northridge earthquake. The MRF exhibits the largest peak displacement (67.8 mm), followed by EBF3 (39.7 mm), while EBF1 and EBF2 demonstrate nearly identical peak values (32.7 mm and 30.9 mm, respectively). Notably, EBF2 shows the most stable post-peak response, with minimal residual displacement due to its concentrated damper arrangement in lower stories. In contrast, EBF3's staggered damper distribution leads to prolonged oscillations, reflecting less efficient energy dissipation. Despite minor variations in peak roof displacements, the braced configurations (EBF1, EBF2, and EBF3) exhibit closely aligned displacement time-history responses, underscoring the consistent kinematic behavior imparted by eccentric bracing systems.

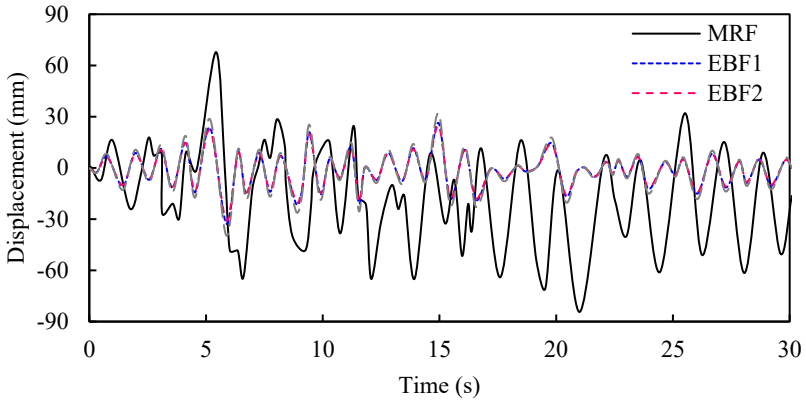

Fig. 11: Roof displacement time histories under Northridge excitation for MRF and EBF configurations

The analysis reveals that the inclusion of eccentrically braced frames provides substantial control over lateral displacements and interstory drifts. Figure 12 presents the profiles of the average maximum story displacement, interstory drift, and story shear for each configuration under all ground motions used in this study at the DBE hazard level. The top story displacement of the EBF1 and EBF2 models was, on average, 36–37% lower than that of the MRF. The EBF2 configuration, with LVSLs concentrated in the lower stories, achieved the lowest peak average interstory drift (0.17%), representing a 43% reduction compared to the MRF. In contrast, the staggered damper arrangement in EBF3 led to a pronounced drift concentration in the second story, validating the concerns identified in the static pushover analysis. This highlights that an irregular vertical distribution of stiffness can induce localized damage, even when the overall system performance is improved relative to an MRF. A statistical summary of the key peak response metrics, including the average, standard deviation, and coefficient of variation across the suite of ground motions, is provided in Table 5. These statistics quantify both the central tendency and the record-to-record variability of the structural response. As expected from their greater stiffness, the EBF configurations attracted higher inertial forces than the MRF, as evidenced by the amplified story shear envelopes in Figure12. While the EBF systems sustained base shears 15-20% higher than the MRF, this increased demand was effectively managed through hysteretic energy dissipation in the LVSLs, a mechanism unavailable to the MRF. The EBF2 configuration proved to be the most effective in this regard, dissipating an average of 81.21% of the input seismic energy. This represents a substantial improvement over both the EBF1 (72.6%) and EBF3 (59.48%) configurations. The superior energy dissipation in EBF2, achieved by strategically placing dampers in the most seismically demanding lower stories, directly corresponds to its enhanced drift control and demonstrates that optimal damper arrangement is critical for maximizing seismic resilience.

5. Comparative Performance under Maximum Considered Earthquake and System Efficiency

To probe the ultimate resilience of the designs, the four configurations were re-analyzed under a maximum considered earthquake (MCE) scenario, simulated by scaling the DBE-level ground motion acceleration histories by a factor of 1.5. This analysis assesses the structures' ability to resist collapse under severe seismic demand. The average maximum interstory drift profiles at the MCE hazard level are presented in Figure 13. As expected, all configurations experienced significantly larger drifts. Nonetheless, the performance hierarchy established under the DBE analysis remained consistent. The EBF systems continued to provide superior drift control compared to the MRF, with the EBF1 and EBF2 configurations performing nearly identically and more effectively than EBF3. The concentration of LVSLs in the lower stories of the EBF2 model again proved beneficial, yielding slightly lower drifts in these critical regions. The staggered damper layout in EBF3 resulted in a persistent and undesirable drift concentration in the second story, reinforcing its inferiority as a design strategy. Beyond seismic

performance, the practical viability of these systems depends on their material efficiency. A weight comparison of the four configurations is detailed in Table 6. While the increased steel tonnage of the EBF systems implies a higher initial material cost, the subsequent discussion demonstrates that this increase should be viewed within a broader life-cycle consideration. Although the EBF systems required approximately 13% more structural steel than the MRF due to the addition of bracing, this investment yielded substantial improvements in stiffness, strength, and drift control.

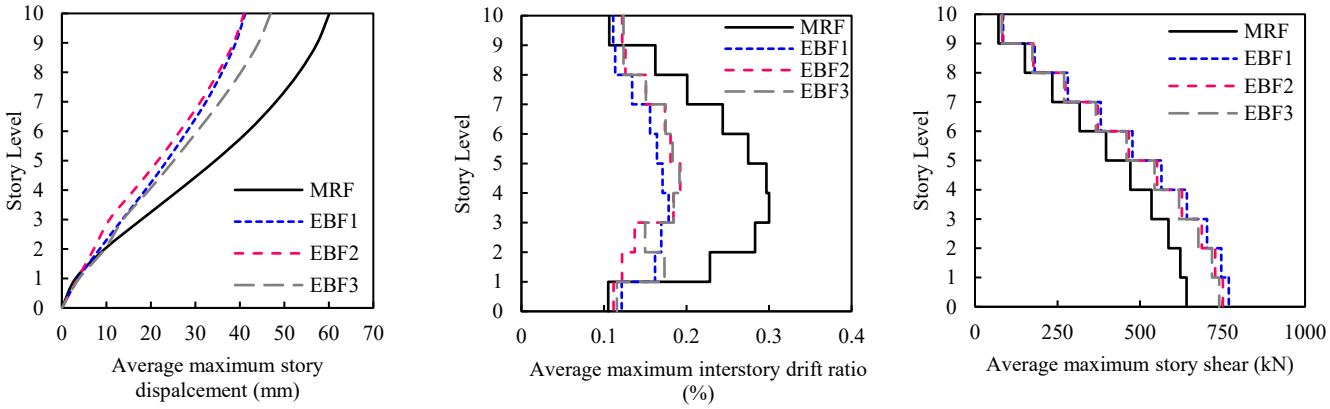

Fig. 12: Profiles of average maximum seismic response at DBE hazard level

Table 5: Statistical summary of peak dynamic response metrics under DBE scenarios

Configuration	Metric	Average	Standard deviation	Coefficient of variance (%)
MRF	Max. base shear (kN)	641	125	19.5
	Max. disp. (mm)	60.12	18.6	31.0
	Peak drift ratio (%)	0.30	0.10	33.3
	Energy diss. ratio (%)	-	-	-
EBF1	Max. base shear (kN)	769	118	15.3
	Max. disp. (mm)	39.07	8.8	22.5
	Peak drift ratio (%)	0.18	0.04	22.2
	Energy diss. ratio (%)	72.60	8.0	11.0
EBF2	Max. base shear (kN)	751	105	14.0
	Max. disp. (mm)	40.94	7.8	19.1
	Peak drift ratio (%)	0.17	0.03	17.6
	Energy diss. ratio (%)	81.21	7.3	9.0
EBF3	Max. base shear (kN)	740	126	17.0
	Max. disp. (mm)	46.96	12.2	26.0
	Peak drift ratio (%)	0.19	0.05	26.3
	Energy diss. ratio (%)	59.48	10.1	17.0

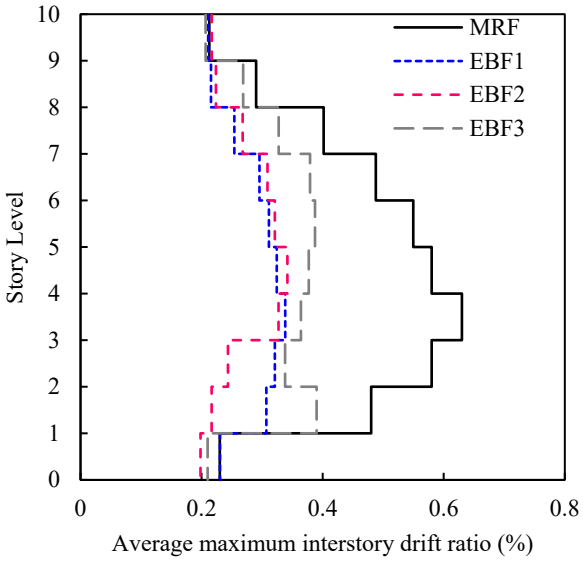

Fig. 13: Average maximum interstory drift ratios at MCE hazard level

Table 6: Weight comparison of structural configurations

Configuration	Structural steel weight (kN)	Stainless steel damper weight (kN)	Total weight (kN)
MRF	252	-	252.00
EBF1	285	0.24	285.24
EBF2	285	0.22	285.22
EBF3	285	0.23	285.23

To quantify the trade-off between material consumption and seismic performance, a seismic efficiency index (I_{SE}) was evaluated for each configuration. The I_{SE} is defined as the percentage reduction in average maximum interstory drift relative to the MRF benchmark per unit of total structural weight (W_{total}). It is expressed as:

$$I_{\mathrm{SE}} = \frac{(\Delta_{\mathrm{MRF}} - \Delta_{\mathrm{EBF}})/\Delta_{\mathrm{MRF}}}{W_{\mathrm{total}}} \times 100 \qquad (3)$$

where Δ_{MRF} and Δ_{EBF} are the peak interstory drift ratios for the MRF and the specific EBF configuration, respectively. Although all EBF configurations utilize an identical amount of structural carbon steel (285 kN) for the primary frame, the variation in link arrangement influences the global efficiency. The EBF2 configuration yields the highest efficiency index ($I_{\mathrm{SE,EBF2}} = 0.152$), which exceeds that of EBF1 ($I_{\mathrm{SE,EBF2}} = 0.140$) and EBF3 ($I_{\mathrm{SE,EBF3}} = 0.129$). This metric confirms that the concentrated damper arrangement (EBF2) provides the most effective kinematic response per unit of material utilized. Consequently, the superior performance of EBF2 is attributed to the strategic placement of dampers rather than an increase in structural mass.

To provide a consolidated graphical summary of these findings, the key performance and efficiency metrics for the EBF configurations are presented and compared in Figure 14. The first two metrics, ultimate strength and peak interstory drift, are normalized with respect to the MRF, which serves as the 100% baseline. For these metrics, a higher strength value is desirable, whereas a lower drift value indicates superior performance. The latter two metrics, energy dissipation and damper weight, are presented to compare the EBF systems relative to each other; higher energy dissipation is favorable, while lower damper weight signifies greater material efficiency. The quantitative comparison in Figure 14 reveals a clear hierarchy of performance. The EBF2 configuration consistently demonstrates the most favorable response, achieving the highest ultimate strength (129% of the MRF) and the greatest reduction in peak interstory drift (to 57% of the MRF value, a reduction of 43%). Furthermore, when comparing the braced systems directly, EBF2 exhibits the highest energy dissipation capacity (81%), substantially outperforming EBF3 (60%). Crucially, this superior performance is achieved with the greatest material efficiency. The EBF2 configuration utilizes the lowest mass of stainless-steel dampers, weighing 8% less than the dampers in the EBF1 arrangement. This graphical synthesis underscores the central finding of the study: a strategic concentration of smaller, more numerous dampers in the lower stories (EBF2) provides an optimal balance, maximizing seismic resilience while simultaneously minimizing the required mass of high-cost damper material.

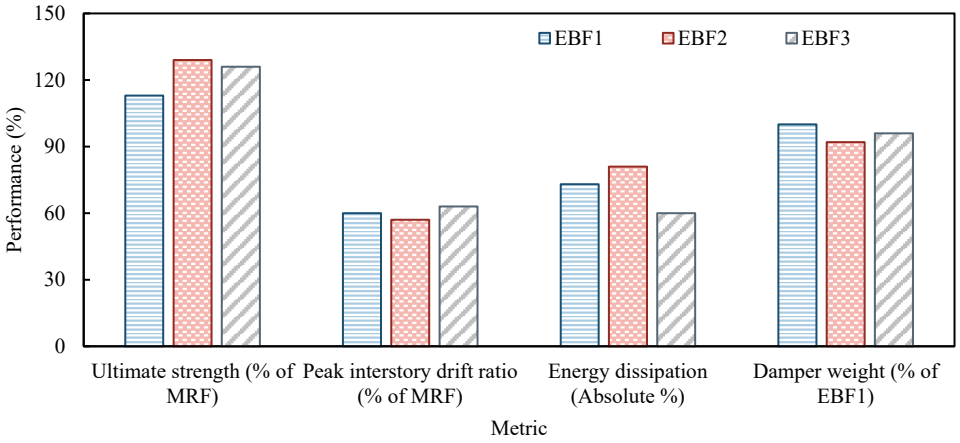

Fig. 14: Comparative summary of key performance and efficiency metrics for the EBF configurations

6. Conclusion

This study presents a systematic investigation into how the arrangement of stainless-steel LVSLs affects the seismic performance of a ten-story steel frame. The key findings from the comparative analyses are as follows:

1. All EBF configurations provided superior seismic performance compared to the benchmark MRF. The optimal EBF configuration (EBF2) reduced the average peak interstory drift by 43% under DBE scenarios and achieved an ultimate strength 22% greater than the MRF in static analysis.
2. A configuration that concentrated two LVSLs in each of the first three stories (EBF2) proved to be the most effective. This arrangement maximized energy dissipation, absorbing 81% of the input seismic energy, which was a significant improvement over the other EBF models. This enhanced dissipation directly translated to the most uniform drift distribution and superior performance under both DBE and MCE scenarios.
3. An irregular or staggered damper arrangement (EBF3) introduced a vertical stiffness discontinuity that led to a detrimental concentration of interstory drift in the second story. This configuration also exhibited reduced energy dissipation capacity, underscoring the importance of maintaining a consistent lateral resistance profile along the building's height.
4. Seismic resilience was achieved with notable material efficiency. The best-performing EBF2 configuration utilized the lowest mass of stainless-steel dampers, weighing 8% less than the next-best arrangement (EBF1). This underscores the critical role of strategic damper placement in achieving both structural safety and material efficiency.
5. Although the optimal EBF configuration entails a higher initial material cost, it presents a compelling case for improved life-cycle performance and resilience. The system's design as a 'structural fuse' enhances reparability and mitigates long-term repair costs, while the use of stainless steel ensures durability and minimizes maintenance requirements, justifying the initial investment.

It is acknowledged that the 2D planar frame analysis presented herein, while suitable for this fundamental comparative study, has inherent limitations. The model does not capture potential torsional effects arising from plan irregularities or bi-directional seismic loading. Additionally, while the use of five spectrally matched ground motions provided a stable estimate of the mean response for this comparative study, future compliance-level design assessments should ideally utilize a suite of at least seven records to fully satisfy code provisions for averaging results. Furthermore, the findings of this study are based on a prototype structure with a fixed bay aspect ratio (story height to beam length) of 0.5 and a design that adheres to capacity design principles. This ensures that the flexural and shear capacity of the members framing the LVSLs (beams and columns) is sufficient to develop the link's full inelastic capacity, consistent with the "strong frame, weak link" philosophy. The influence of varying the beam-to-column stiffness ratio and its effect on the optimal damper arrangement was beyond the scope of this investigation. Consequently, future research should prioritize the development of three-dimensional models to evaluate the influence of LVSL arrangements on torsional response and should include parametric studies to assess the generality of these findings across a wider range of frame geometries. A comprehensive life-cycle cost analysis, considering factors such as fabrication complexity and post-earthquake

reparability, would also provide valuable data to guide practical implementation.

Acknowledgement

This work has been financially supported by the Vice-Chancellor for Research of the University of Torbat-e Jam and the China Scholarship Council (CSC) through grants 2024GSP006483 and 2024GSP006413. The authors express their sincere gratitude for this support, which has been instrumental in facilitating the research presented in this paper.

References

[1] Li H, Qi Y, Kang T, Wang H. Study on Lateral-Load Resisting Mechanism and Capacities of Steel Frame Infilled with Composite Plate Shear Wall Under Cyclic Loading. Materials 2025;18:1677. https://doi.org/10.3390/ma18071677.

[2] Nurjannah SA, Rosidawani, Saloma, Hanafiah, Rafly M. Performance-based Analysis of Building Structures in Various Earthquake Zones. IOP Conf Ser: Earth Environ Sci 2023;1244:012019. https://doi.org/10.1088/1755-1315/1244/1/012019.

[3] Tartaglia R, D'Aniello M, Maddaloni G, Landolfo R. Seismic Performance of Moment-Resisting–Eccentrically Braced Dual Frame Equipped with Detachable Links. Applied Sciences 2024;14:4676. https://doi.org/10.3390/app14114676.

[4] Popov EP. Seismic Steel Framing Systems for Tall Buildings. Eng J 1982;19:141–9. https://doi.org/10.62913/engj.v19i3.385.

[5] Arum C, Akinkunmi A. Comparison of Wind-Induced Displacement Characteristics of Buildings with Different Lateral Load Resisting Systems. ENG 2011;03:236–47. https://doi.org/10.4236/eng.2011.33028.

[6] Longo A, Montuori R, Piluso V. Moment frames – concentrically braced frames dual systems: analysis of different design criteria. Structure and Infrastructure Engineering 2016;12:122–41. https://doi.org/10.1080/15732479.2014.996164.

[7] Hu S, Wang W, Qu B. Seismic economic losses in mid-rise steel buildings with conventional and emerging lateral force resisting systems. Engineering Structures 2020;204:110021. https://doi.org/10.1016/j.engstruct.2019.110021.

[8] Titirla MD. A State-of-the-Art Review of Passive Energy Dissipation Systems in Steel Braces. Buildings 2023;13:851. https://doi.org/10.3390/buildings13040851.

[9] Elgammal A, El-Khoriby S, Seleemah A. Seismic Retrofitting of Existing Reinforced Concrete Buildings Using Aluminium Shear Links and Eccentric Steel Chevron Braces. Arab J Sci Eng 2024;49:1–35. https://doi.org/10.1007/s13369-024-08908-8.

[10] Di Cesare A, Ponzo FC. Seismic Retrofit of Reinforced Concrete Frame Buildings with Hysteretic Bracing Systems: Design Procedure and Behaviour Factor. Shock and Vibration 2017;2017:1–20. https://doi.org/10.1155/2017/2639361.

[11] Di Cesare A, Ponzo FC, Nigro D. Assessment of the performance of hysteretic energy dissipation bracing systems. Bull Earthquake Eng 2014;12:2777–96. https://doi.org/10.1007/s10518-014-9623-z.

[12] Phocas MC, Sophocleous TL. Adaptable dual control systems. A comparative parametric analysis. Int J of Safety and Security Eng 2012;2:280–96. https://doi.org/10.2495/SAFE-V2-N3-280-296.

[13] Elgammal A, Ali Y. A novel hysteretic restoring force model for shear link dampers: A machine learning approach. Structures 2024;70:107848. https://doi.org/10.1016/j.istruc.2024.107848.

[14] Elgammal A, Hassanein MF, Seleemah A. Enhancing the cyclic performance of shear links using longitudinal stiffeners. Journal of Constructional Steel Research 2023;211:108200. https://doi.org/10.1016/j.jcsr.2023.108200.

[15] Ghobarah A, Ramadan T. Seismic analysis of links of various lengths in eccentrically braced frames. Can J Civ Eng 1991;18:140–8. https://doi.org/10.1139/l91-016.

[16] Wen H, Mahmoud H. A New Approach to Predict Cyclic Response and Fracture of Shear Links and Eccentrically Braced Frames. Front Built Environ 2018;4:11. https://doi.org/10.3389/fbuil.2018.00011.

[17] Yao Z, Wang W, Fang C, Zhang Z. An experimental study on eccentrically braced beam-through steel frames with replaceable shear links. Engineering Structures 2020;206:110185. https://doi.org/10.1016/j.engstruct.2020.110185.

[18] Ashrafi A, Imanpour A. Seismic response of steel multi-tiered eccentrically braced frames. Journal of Constructional Steel Research 2021;181:106600. https://doi.org/10.1016/j.jcsr.2021.106600.

[19] Aied Qissab Al-Janabi M, Topkaya C. Seismic performance of eccentrically braced frames designed to AISC341 and EC8 specifications. Structures 2021;29:339–59. https://doi.org/10.1016/j.istruc.2020.11.031.

[20] Miao F, Nejati F, Zubair SAM, Yassin ME. Seismic Performance of Eccentrical Braced Frame Retrofitted by Box Damper in Vertical Links. Buildings 2022;12:1506. https://doi.org/10.3390/buildings12101506.

[21] Rai DC, Wallace BJ. Aluminium shear-links for enhanced seismic resistance. Earthquake Engng Struct Dyn 1998;27:315–42. https://doi.org/10.1002/(SICI)1096-9845(199804)27:4<315::AID-EQE703>3.0.CO;2-N.

[22] Shayanfar MA, Barkhordari MA, Rezaeian AR. Experimental study of cyclic behavior of composite vertical shear link in eccentrically braced frames. Steel and Composite Structures 2012;12:13–29. https://doi.org/10.12989/SCS.2012.12.1.013.

[23] Hu S, Liu S, Xu H, Zeng S, Zhang B, Yu Y. Experimental investigation of an innovative very short shear link with shear slotted bolted connection in eccentrically braced frames. Structures 2024;66:106890. https://doi.org/10.1016/j.istruc.2024.106890.

[24] Huangfu S-E, Tao Z, Zhang Y, Yuan Z, Li H, Zhang Z. Web tension field action of a stainless steel section with stiffened web and folded flanges under bending and shear interaction. Sci Rep 2025;15:5146. https://doi.org/10.1038/s41598-025-89314-4.

[25] Huangfu S-E, Tao Z, Zhang Z, Wang Z, Zhang J. Numerical Study on the Shear Behavior of a Late-Model Cold-Formed Stainless Steel C-Shaped Beam. Materials 2024;18:91. https://doi.org/10.3390/ma18010091.

[26] Elgammal A, Ali Y. Optimizing stiffener orientation in cold-formed shear panel dampers for enhanced ductility and energy dissipation. Asian J Civ Eng 2025. https://doi.org/10.1007/s42107-025-01398-5.

[27] Lázaro L, Chacón R. Material behaviour of austenitic stainless steel subjected to cyclic and arbitrary loading. Journal of Constructional Steel Research 2022;189:107113. https://doi.org/10.1016/j.jcsr.2021.107113.

[28] Duan H, Cao M, Liu L, Yue S, He H, Zhao Y, Zhang Z, Liu Y. Prediction of 316 stainless steel low-cycle fatigue life based on machine learning. Sci Rep 2023;13:6753. https://doi.org/10.1038/s41598-023-33354-1.

[29] Duan H, Yue S, Liu Y, He H, Zhang Z, Zhao Y. A deep learning-based method for predicting the low-cycle fatigue life of austenitic stainless steel. Mater Res Express 2023;10:086506. https://doi.org/10.1088/2053-1591/aced39.

[30] Bao S, Feng H, Song Z, He J, Wu X, Gu Y. Study on the Deformation Behavior of Two Phases during the Low Cycle Fatigue of UNS S32750 Duplex Stainless Steel. Materials 2024;17:3390. https://doi.org/10.3390/ma17143390.

[31] Zheng S, Zhou F, Cheng J, Li H-T, Rong R. Experimental study on cyclic hardening characteristics of structural stainless steels. Journal of Constructional Steel Research 2022;191:107196. https://doi.org/10.1016/j.jcsr.2022.107196.

[32] Pate SB, Dundulis G, Griskevicius P. Modeling of LCF Behaviour on AISI316L Steel Applying the Armstrong–Frederick Kinematic Hardening Model. Materials 2024;17:3395. https://doi.org/10.3390/ma17143395.

[33] Hu Y, Tang S, Liu Y, Li L, Wang C, Wang Q. The Gradient Effect on Cyclic Behavior of 316L Stainless Steel in the Ultrasonic Bending Test. Materials 2024;17:1657. https://doi.org/10.3390/ma17071657.

[34] Hwang B, Kim T, Ahn Y. Experimental investigation of structural behavior of 316L stainless steel and carbon steel slit dampers. Thin-Walled Structures 2023;186:110704. https://doi.org/10.1016/j.tws.2023.110704.

[35] Zhao J, Luo J, Zhang X, Ruan X, Sun Y. Experimental study on seismic behavior of concrete walls with external magnetorheological dampers. Smart Mater Struct 2023;32:065005. https://doi.org/10.1088/1361-665X/accd31.

[36] Ramanjaneyulu B, Prasad A, Satish K, Keertan TS, Bommisetty J. Seismic analysis of vertically irregular RCC high-rise buildings: A study with provision of FVD at various locations. IOP Conf Ser: Earth Environ Sci 2024;1409:012034. https://doi.org/10.1088/1755-1315/1409/1/012034.

[37] Kurucu MC, Atam E, Güzelkaya M, Eksin İ. Intelligent Computational Methods for Optimal Distribution of Friction Dampers in Seismic Protection of Buildings. IEEE Trans Emerg Top Comput Intell 2024;8:3055–66. https://doi.org/10.1109/TETCI.2024.3369909.

[38] Dong S, Pan W, Ye L, Wang J. Design of displacement-based viscous damper damping structures. Sci Rep 2025;15:11742. https://doi.org/10.1038/s41598-025-94016-y.

[39] Javaid K, Verma N. Vibration control of seismic forces using viscous dampers and buckling restrained braces in irregular composite buildings. IOP Conf Ser: Earth Environ Sci 2023;1110:012052. https://doi.org/10.1088/1755-1315/1110/1/012052.

[40] European Committee for Standardization (CEN). Eurocode 3: Design of steel structures-Part 1–1: General rules and rules for buildings 2005.

[41] European Committee for Standardization (CEN). Eurocode 8: Design of structures for earthquake resistance - Part 1: General rules, seismic actions and rules for buildings 2004.

[42] Elgammal A. Improving the Performance of Vertical Shear Links for Enhanced Seismic Energy Dissipation. MSc Thesis. Tanta University, 2021.

[43] Computers and Structures, Inc. ETABS Ultimate 20.0.0 2021.

[44] American Society of Civil Engineeris (ASCE). Seismic Evaluation and Retrofit of Existing Buildings 2017.

[45] Selemah A, El-Khoriby S, El-Gammal A. Seismic Response of 2-D Plane Framed Buildings Eccentrically Braced with Vertical Shear Links. International Journal of Advances in Structural and Geotechnical Engineering 2022;03:1–18. https://doi.org/10.21608/asge.2022.152698.1006.

[46] Maniyar SU, Paul DK. Enhancement of Seismic Performance Using Shear Link Braces in a Building Designed Only for Gravity Loads. J Inst Eng India Ser A 2012;93:27–43. https://doi.org/10.1007/s40030-012-0005-8.

[47] Lian M, Su M. Seismic performance of high-strength steel fabricated eccentrically braced frame with vertical shear link. Journal of Constructional Steel Research 2017;137:262–85. https://doi.org/10.1016/j.jcsr.2017.06.022.

[48] ANSYS, Inc. ANSYS 2023.

[49] Wen Y-K. Method for Random Vibration of Hysteretic Systems. J Engrg Mech Div 1976;102:249–63. https://doi.org/10.1061/JMCEA3.0002106.

[50] Seismosoft Ltd. SeismoMatch 2025 2025.

[51] Hancock J, Watson-Lamprey J, Abrahamson NA, Bommer∗ JJ, Markatis A, McCOYH E, Mendis R. An improved method of matching response spectra of recorded earthquake ground motion using wavelets. Journal of Earthquake Engineering 2006;10:67–89. https://doi.org/10.1080/13632460609350629.